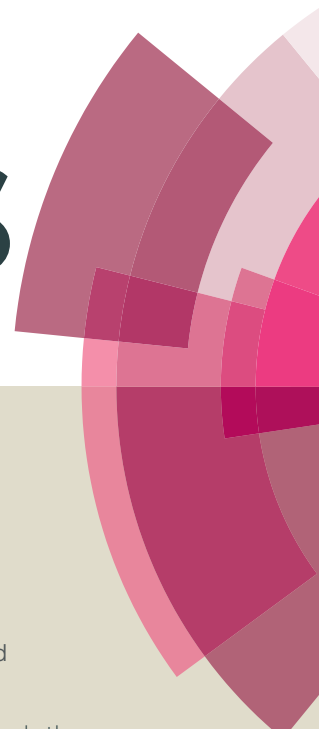


# RSC Advances



This article can be cited before page numbers have been issued, to do this please use: A. Bamoniri and N. Moshtael-Arani, *RSC Adv.*, 2015, DOI: 10.1039/C4RA12604A.



This is an *Accepted Manuscript*, which has been through the Royal Society of Chemistry peer review process and has been accepted for publication.

*Accepted Manuscripts* are published online shortly after acceptance, before technical editing, formatting and proof reading. Using this free service, authors can make their results available to the community, in citable form, before we publish the edited article. This *Accepted Manuscript* will be replaced by the edited, formatted and paginated article as soon as this is available.

You can find more information about *Accepted Manuscripts* in the [Information for Authors](#).

Please note that technical editing may introduce minor changes to the text and/or graphics, which may alter content. The journal's standard [Terms & Conditions](#) and the [Ethical guidelines](#) still apply. In no event shall the Royal Society of Chemistry be held responsible for any errors or omissions in this *Accepted Manuscript* or any consequences arising from the use of any information it contains.

Cite this: DOI: 10.1039/c0xx00000x

www.rsc.org/xxxxxx

## ARTICLE TYPE

# Nano-Fe<sub>3</sub>O<sub>4</sub> encapsulated-silica supported boron trifluoride as a novel heterogeneous solid acid for solvent-free synthesis of arylazo-1-naphthol derivatives

Abdolhamid Bamoniri\* and Naimeh Moshtael-Arani

Received (in XXX, XXX) Xth XXXXXXXXX 20XX, Accepted Xth XXXXXXXXX 20XX

DOI: 10.1039/b000000x

Nano-Fe<sub>3</sub>O<sub>4</sub> encapsulated-silica supported boron trifluoride (Fe<sub>3</sub>O<sub>4</sub>@SiO<sub>2</sub>-BF<sub>3</sub>) as a new type of green heterogeneous solid acid was prepared by the immobilization of BF<sub>3</sub>·Et<sub>2</sub>O on the surface of Fe<sub>3</sub>O<sub>4</sub>@SiO<sub>2</sub> core-shell nanoparticles and characterized by Fourier transform-infrared spectroscopy (FT-IR), X-ray diffraction (XRD), vibrating sample magnetometer (VSM), field emission-scanning electron microscope (FE-SEM), energy dispersive X-ray (EDS), and transmission electron microscope (TEM). Then, this super solid acid as an acidic reagent was used for the synthesis of aryl diazonium salts as a starting reactant and following, their diazo coupling with 1-naphthol in a basic solvent-free medium at room temperature. Main advantages of this clean method were high yields, short reaction times, room temperature, no need to corrosive and toxic liquid acids and solvents. In addition, long-term stability of aryl diazonium salts supported on Fe<sub>3</sub>O<sub>4</sub>@SiO<sub>2</sub>-BF<sub>3</sub> magnetic nanoparticles (MNPs) at room temperature was one of the most important results of this procedure.

## Introduction

In recent years, solvent-free organic reactions<sup>1</sup> have captured great interest because of their many advantages such as high efficiency and selectivity, easy separation and purification, mild reaction condition, reduction in waste, simplicity in progress and handling, and benefit to the industry as well as the environment. Aromatic azo compounds constitute a very important class of organic dyes because of their widespread applications in many areas of technology and medicine. They are well known for their use as colorants in the textile industries,<sup>2</sup> digital printing and photography.<sup>3</sup> They are also applied as chiral receptors,<sup>4</sup> liquid crystals,<sup>5</sup> new glassy materials,<sup>6</sup> chiral switches in photochemistry,<sup>7</sup> dyes for drug, food, cosmetic, biomedicine,<sup>8</sup> and molecular recognition.<sup>9</sup> As synthesis of azo dyes requires some special conditions such as low temperature and concentrated liquid acid, in addition to high costs, it leads to corrosion of reactors and equipments, too.<sup>10</sup> Nowadays, solid supported reagents have resolved these problems and improved activity and selectivity rather than individual reagents.<sup>11</sup> Such reagents not only simplify purification processes but they also help prevent release of reaction residues into the environment.<sup>12</sup> In this regard, nano structure solid acids exhibit higher activity and selectivity than their corresponding bulk materials due to their particular physical and chemical properties especially large surface to

volume ratio.<sup>13</sup> Recently, Fe<sub>3</sub>O<sub>4</sub> MNPs has appeared as a new kind of efficient catalyst support due to low toxicity, ease of surface modification, unique physical properties including the high surface area and superparamagnetism.<sup>14</sup> In order to prevent the aggregation of Fe<sub>3</sub>O<sub>4</sub> nanoparticles, its surface is usually modified with silica layer, taking advantage of being biocompatible and hydrophilic and, also, because the surface silanol groups can easily react with various organic and inorganic materials to achieve the certain purposes especially in the field of catalysis.<sup>15</sup> As a continuation of our efforts on the development of heterogeneous solid acids in organic transformations,<sup>16</sup> we herein report the preparation and characterization of a novel and eco-friendly magnetic solid acid as Fe<sub>3</sub>O<sub>4</sub>@SiO<sub>2</sub>-BF<sub>3</sub> and its utility for the synthesis of arylazo-1-naphthol dyes in a solvent-free environment at room temperature. In this method, it is not require providing special cold condition for stabilization of aryl diazonium salt. The reaction easily takes place at room temperature and resulting diazonium salt can remain on the solid substrate for several months. To the best of our knowledge, this research is the first report about long-term stability of aryl diazonium salts supported on the surface of MNPs and their use as the reactant for synthesis of arylazo-1-naphthols in solvent-free condition. The findings of this research may have implications for

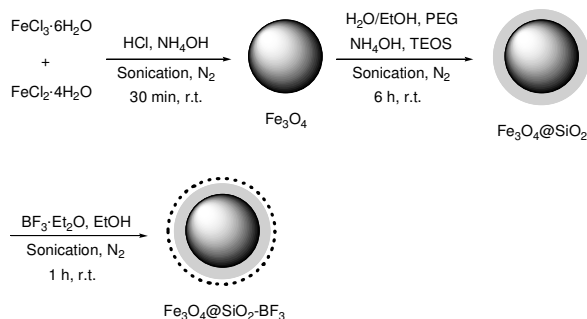
effective synthesis on a larger scale in dyeing and medical industries.

## Results and discussion

This research was performed in three stages. Initially,  $\text{Fe}_3\text{O}_4@/\text{SiO}_2\text{--BF}_3$  MNPs was synthesized and identified by FT-IR, XRD, VSM, FE-SEM, EDS, and TEM. In the second stage, aryl diazonium salts were synthesized in the presence of  $\text{Fe}_3\text{O}_4@/\text{SiO}_2\text{--BF}_3$  nanoparticles at room temperature and their structure and stability was investigated. The third stage was diazo coupling of aryl diazonium salts supported on  $\text{Fe}_3\text{O}_4@/\text{SiO}_2\text{--BF}_3$  with basic 1-naphthol under solvent-free grinding condition.

### Synthesis and characterization of $\text{Fe}_3\text{O}_4@/\text{SiO}_2\text{--BF}_3$ nanoparticles

$\text{Fe}_3\text{O}_4@/\text{SiO}_2\text{--BF}_3$  core-shell nanoparticles, with  $\text{Fe}_3\text{O}_4$  spheres as the core and silica supported  $\text{BF}_3$  as the shell, was prepared by a simple and convenient method. At first,  $\text{Fe}_3\text{O}_4$  nanoparticles were prepared by chemical co-precipitation of  $\text{FeCl}_2\cdot 4\text{H}_2\text{O}$  and  $\text{FeCl}_3\cdot 6\text{H}_2\text{O}$  in ammonium hydroxide solution. To improve the chemical stability of  $\text{Fe}_3\text{O}_4$  and prevent self-aggregation, its surface engineering was successfully performed by the suitable deposition of  $\text{SiO}_2$  onto  $\text{Fe}_3\text{O}_4$  surface via the ammonia-catalyzed hydrolysis of tetraethylorthosilicate (TEOS). Next, the  $\text{Fe}_3\text{O}_4@/\text{SiO}_2$  spheres served as support for the immobilization of  $\text{BF}_3$  groups by simple stirring of  $\text{Fe}_3\text{O}_4@/\text{SiO}_2$  and  $\text{BF}_3\cdot\text{Et}_2\text{O}$  in ethanol. All three steps were carried out under sonication condition at room temperature (Scheme 1).



**Scheme 1** Preparation of  $\text{Fe}_3\text{O}_4@/\text{SiO}_2\text{--BF}_3$  MNPs under sonication condition at room temperature.

In order to identify the molecular structures of  $\text{Fe}_3\text{O}_4$ ,  $\text{Fe}_3\text{O}_4@/\text{SiO}_2$ , and  $\text{Fe}_3\text{O}_4@/\text{SiO}_2\text{--BF}_3$  MNPs, FT-IR analysis of three mentioned samples was performed (Fig. 1).  $\text{Fe}_3\text{O}_4$  was identified by a stretching vibration of the Fe–O absorption peak at  $576\text{ cm}^{-1}$ , O–H stretching vibration at  $3429\text{ cm}^{-1}$  and O–H deformed vibration at  $1625\text{ cm}^{-1}$  in Fig. 1a. The FT-IR spectrum of  $\text{Fe}_3\text{O}_4@/\text{SiO}_2$  (Fig. 1b) displayed characteristic peaks at  $1093$  and  $800\text{ cm}^{-1}$  corresponding to symmetrical and asymmetrical vibrations of Si–O–Si, respectively. Weak band at  $466\text{ cm}^{-1}$  corresponded to the Si–O–Fe stretching vibrations of the  $\text{Fe}_3\text{O}_4@/\text{SiO}_2$  core-shell, overall confirming the presence of  $\text{SiO}_2$  in the sample. The successful covalent linking of the  $\text{BF}_3\cdot\text{Et}_2\text{O}$  on the surface of  $\text{Fe}_3\text{O}_4@/\text{SiO}_2$  core-shell was proved by the appearance of a new band at  $1457\text{ cm}^{-1}$ , which originates

from the absorption of B–O (Fig. 1c). The absorption band of B–F was hidden under Si–O band. Also, the ethanolic OH and existing moisture in  $\text{BF}_3\cdot\text{Et}_2\text{O}$  caused a broad O–H stretching band at wavenumber of  $3221\text{ cm}^{-1}$ . Again observation of  $\text{Fe}_3\text{O}_4$  absorption peaks in Fig. 1b and Fig. 1c implies that  $\text{Fe}_3\text{O}_4$  MNPs do not change chemically or physically after coating and surface modification processes. According to this information and regarding the reported structure of  $\text{BF}_3\cdot\text{SiO}_2$  in the literature,<sup>17</sup> the final structure of nano  $\text{Fe}_3\text{O}_4@/\text{SiO}_2\text{--BF}_3$  was predicted in Scheme 2.

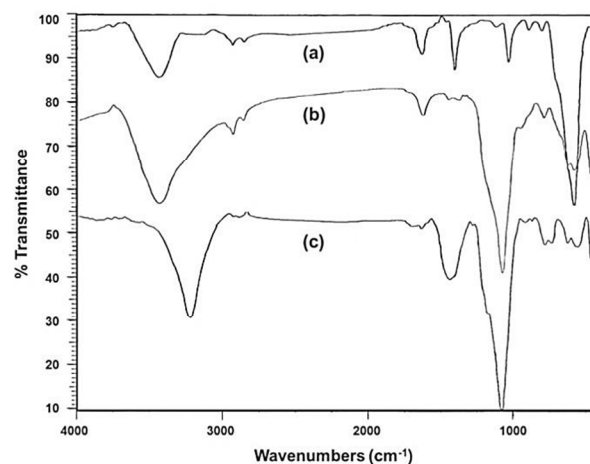
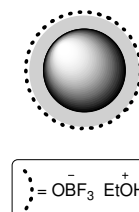


**Fig. 1** FT-IR spectra of a)  $\text{Fe}_3\text{O}_4$ , b)  $\text{Fe}_3\text{O}_4@/\text{SiO}_2$  and c)  $\text{Fe}_3\text{O}_4@/\text{SiO}_2\text{--BF}_3$ .



**Scheme 2** The structure of  $\text{Fe}_3\text{O}_4@/\text{SiO}_2\text{--BF}_3$  MNPs.

Fig. 2 shows the XRD powder diffraction patterns of three synthesized MNPs. The data for the  $\text{Fe}_3\text{O}_4$  nanoparticles at  $2\theta$  of  $30.22$ ,  $35.61$ ,  $43.25$ ,  $53.58$ ,  $57.30$ ,  $62.89$ , and  $74.66^\circ$  (Fig. 2a) corresponded to the standard  $\text{Fe}_3\text{O}_4$  powder diffraction data. Moreover, the relatively sharp peaks observed indicate phase purity of  $\text{Fe}_3\text{O}_4$  nanoparticles, which are consistent with the presence of the cubic inverse spinel structure of  $\text{Fe}_3\text{O}_4$ . The XRD pattern of the  $\text{Fe}_3\text{O}_4@/\text{SiO}_2$  (Fig. 2b) was in good agreement with that of  $\text{Fe}_3\text{O}_4$  phase, except for a broad peak around  $2\theta$  of  $20\text{--}30^\circ$  corresponding to amorphous phase of  $\text{SiO}_2$ . This indicates that the MNPs obtained after the coating process are composed of  $\text{Fe}_3\text{O}_4$  core and amorphous  $\text{SiO}_2$  shell. The XRD pattern of the modified  $\text{Fe}_3\text{O}_4@/\text{SiO}_2$  with  $\text{BF}_3\cdot\text{Et}_2\text{O}$  in Fig. 2c was nearly the same with Fig. 2b, which it seems that the surface modification by  $\text{BF}_3$  group has little effect on the XRD pattern of  $\text{Fe}_3\text{O}_4@/\text{SiO}_2$  nanoparticles, because of the shielding effect of  $\text{Fe}_3\text{O}_4$  and  $\text{SiO}_2$  peaks. However, the changes in peaks intensity in spectra 2b and 2c and increase the noise in Fig. 2c can verify the linking of  $\text{BF}_3$  on the surface of  $\text{Fe}_3\text{O}_4@/\text{SiO}_2$  core-shell MNPs. Furthermore, characteristic peaks of  $\text{Fe}_3\text{O}_4$  were observed in three samples, thereby

indicating that the binding process did not induce any phase change.

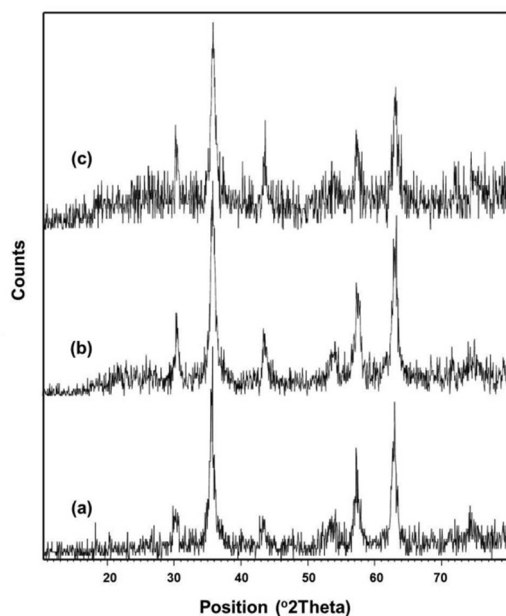


**Fig. 2** XRD patterns of (a)  $\text{Fe}_3\text{O}_4$ , (b)  $\text{Fe}_3\text{O}_4@\text{SiO}_2$ , and (c)  $\text{Fe}_3\text{O}_4@\text{SiO}_2\text{-BF}_3$ .

The magnetic properties of synthesized  $\text{Fe}_3\text{O}_4$ ,  $\text{Fe}_3\text{O}_4@\text{SiO}_2$ , and  $\text{Fe}_3\text{O}_4@\text{SiO}_2\text{-BF}_3$  nanoparticles were assessed by VSM at room temperature. The magnetization curve in Fig. 3 indicates magnetization as a function of applied magnetic field. The saturation magnetization of the  $\text{Fe}_3\text{O}_4@\text{SiO}_2$  nanoparticles in Fig. 3b was about 29.15 emu/g, and this reduced to 27.44 emu/g after supporting with  $\text{BF}_3\cdot\text{Et}_2\text{O}$  (Fig. 3c). Both of these values were much lower than the initial saturation magnetization of  $\text{Fe}_3\text{O}_4$  nanoparticles (59.2 emu/g) in Fig. 3a. The decrease of the saturation magnetization after surface coating of  $\text{Fe}_3\text{O}_4$  confirms the presence of a diamagnetic outer shell ( $\text{SiO}_2$  or  $\text{SiO}_2\text{-BF}_3$ ) at the surface of the  $\text{Fe}_3\text{O}_4$  particles.

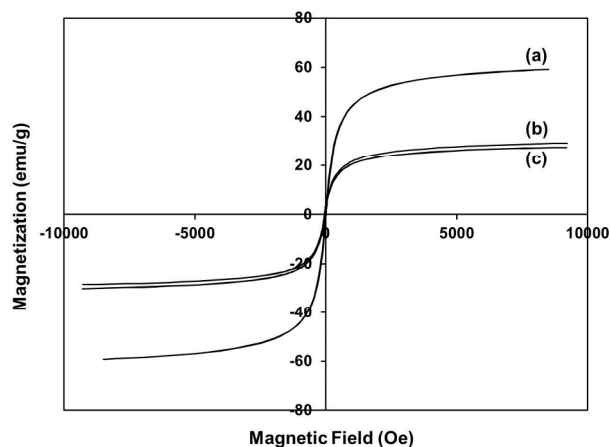


**Fig. 3** Magnetization curves of (a)  $\text{Fe}_3\text{O}_4$ , (b)  $\text{Fe}_3\text{O}_4@\text{SiO}_2$ , and (c)  $\text{Fe}_3\text{O}_4@\text{SiO}_2\text{-BF}_3$ .

The high magnification FE-SEM images of the purified MNPs are displayed in Fig. 4(a-c). These images clearly showed the

surface morphology of three kinds of synthesized MNPs with a nearly spherical shape. Elemental components of three MNPs were characterized by EDS analysis. Fig. 4d shows EDS of the  $\text{Fe}_3\text{O}_4$  nanoparticles, in which the particles contain Fe and O elements. The presence of Fe, O and Si elements in Fig. 4e verified the coating of  $\text{Fe}_3\text{O}_4$  core by  $\text{SiO}_2$  shell. The appearance of two new signals related to F and C elements in Fig. 4f confirmed supporting of  $\text{BF}_3\cdot\text{Et}_2\text{O}$  on  $\text{Fe}_3\text{O}_4@\text{SiO}_2$  core-shell nanoparticles according to Scheme 2.

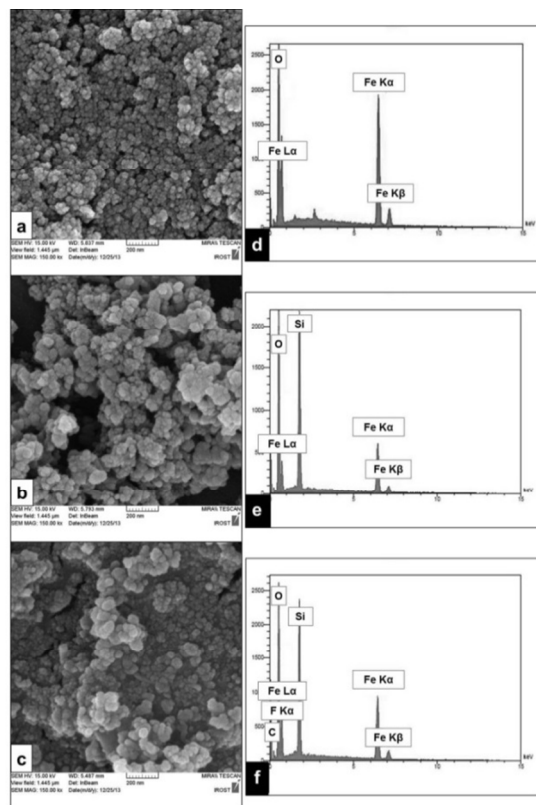


**Fig. 4** FE-SEM images of (a)  $\text{Fe}_3\text{O}_4$ , (b)  $\text{Fe}_3\text{O}_4@\text{SiO}_2$ , (c)  $\text{Fe}_3\text{O}_4@\text{SiO}_2\text{-BF}_3$  and EDS spectra of (d)  $\text{Fe}_3\text{O}_4$ , (e)  $\text{Fe}_3\text{O}_4@\text{SiO}_2$ , (f)  $\text{Fe}_3\text{O}_4@\text{SiO}_2\text{-BF}_3$ .

TEM images of  $\text{Fe}_3\text{O}_4$  and  $\text{Fe}_3\text{O}_4@\text{SiO}_2\text{-BF}_3$  are displayed in Fig. 5. As demonstrated in Fig. 5a,  $\text{Fe}_3\text{O}_4$  nanoparticles have the spherical morphology. In Fig. 5b, two regions with different electron densities can be distinguished that confirms the  $\text{Fe}_3\text{O}_4$  nanoparticles were successfully coated with a thin layer of a different phase. However, it can be observed that the sample is nearly in core-shell structure. An electron dense region (black colour) which corresponds to  $\text{Fe}_3\text{O}_4$  cores and a less dense or more translucent region (ash colour) surrounding these cores that is  $\text{SiO}_2\text{-BF}_3$  shell. From the size distribution histograms, the average size of 9 nm for  $\text{Fe}_3\text{O}_4$  and 13 nm for  $\text{Fe}_3\text{O}_4@\text{SiO}_2\text{-BF}_3$  nanoparticles could be estimated.



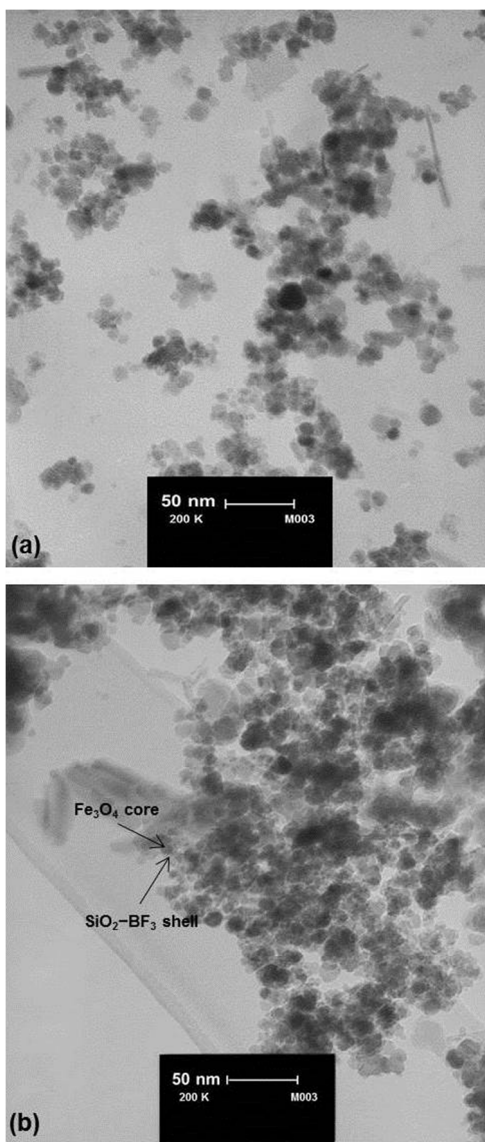


**Fig. 5** TEM images of (a)  $\text{Fe}_3\text{O}_4$ , and (b)  $\text{Fe}_3\text{O}_4@\text{SiO}_2\text{-BF}_3$  nanoparticles.

Finally,  $\text{Fe}_3\text{O}_4@\text{SiO}_2\text{-BF}_3$  was identified by using the techniques described above, and applied for synthesis of arylazo-1-naphthol derivatives.

### Synthesis and characterization of aryl diazonium salts

Aryl diazonium salts are usually synthesized in the presence of a liquid acid dissolved in water at low temperatures between 0 to 5 °C, because temperatures above 5 °C generally promote phenol formation in aqueous media. Thus, as synthesis of aryl diazonium salts has limitations and drawbacks such as the control and maintenance of the low-temperature, using toxic liquid acids that are incompatible with environment, and most important of all, instability of aryl diazonium salts at room temperature, we tried to resolve these problems by the development a green and simple procedure for synthesis of aryl diazonium salts and in continue, their diazo coupling with 1-naphthol.

At first, in order to evaluate the efficiency of  $\text{Fe}_3\text{O}_4@\text{SiO}_2\text{-BF}_3$  MNPs in diazotization reaction, an initial optimization of the kind and amount of acidic reagent was performed via

diazotization of 4-chloro aniline as a model substrate. A range of parameters such as stability of 4-chlorophenyl diazonium salt at room temperature, reaction time of diazotization, and yield of resulted 4-chlorophenylazo-1-naphthol were screened in Table 1.

Solid acids such as silica phosphoric acid and silica chloride gave the 4-chlorophenylazo-1-naphthol with modest yields of 57% and 61%, respectively (Table 1, entries 1 and 2). The stability of aryl diazonium salt supported on above mentioned solid acids was maximum 2 days.  $\text{Fe}_3\text{O}_4@\text{SiO}_2$  and  $\text{BF}_3\cdot\text{Et}_2\text{O}$  sources were also tested individually. There was no reaction in the presence of neither  $\text{Fe}_3\text{O}_4@\text{SiO}_2$  nor  $\text{BF}_3\cdot\text{Et}_2\text{O}$  (Table 1, entries 3 and 4), while  $\text{Fe}_3\text{O}_4@\text{SiO}_2\text{-BF}_3$  with different loadings afforded the improved yields from 87% to 95% for 4-chlorophenylazo-1-naphthol (Table 1, entries 5-8). These results clearly indicated that the presence of Brønsted acid sites on the solid acid surface is essential for promoting diazotization. Also, the rate of diazotization in the presence of  $\text{Fe}_3\text{O}_4@\text{SiO}_2\text{-BF}_3$  MNPs was much higher than silica phosphoric acid and silica chloride.

In another comparative study (Table 1, entries 5-8), the effect of  $\text{Fe}_3\text{O}_4@\text{SiO}_2$  loading by  $\text{BF}_3\cdot\text{Et}_2\text{O}$  on the acidic performance of  $\text{Fe}_3\text{O}_4@\text{SiO}_2\text{-BF}_3$  was investigated. Although the time of diazotization and the stability of aryl diazonium salt supported on  $\text{Fe}_3\text{O}_4@\text{SiO}_2\text{-BF}_3$  nanoparticles with different loadings in the same conditions were approximately identical, but 10 wt%  $\text{Fe}_3\text{O}_4@\text{SiO}_2\text{-BF}_3$  resulted in the highest yield of the corresponding azo dye (Table 1, entry 6). In conclusion, 10 wt%  $\text{Fe}_3\text{O}_4@\text{SiO}_2\text{-BF}_3$  was selected as the most ideal acid for synthesis of arylazo-1-naphthol dyes among those listed in Table 1.

In addition, with more investigations, it was found that aryl diazonium salts supported on  $\text{Fe}_3\text{O}_4@\text{SiO}_2\text{-BF}_3$  nanoparticles underwent no significant change at room temperature for several months. To explore the reason of this unusual stability, FT-IR spectrum of 4-chlorophenyl diazonium salt was studied (Fig. 6).

**Table 1** Comparison of efficiency of various acids in synthesis of 4-chlorophenyl diazonium salt.

Entry	Acid (wt %)			
		Stability at r.t.	Time of diazotization	Yield <sup>a</sup> (%)
1	SPA <sup>b</sup> (10)	~ 2 days	35 min	57
2	SC <sup>c</sup> (10)	~ 2 days	30 min	61
3	$\text{Fe}_3\text{O}_4@\text{SiO}_2$	---	No reaction	---
4	$\text{BF}_3\cdot\text{Et}_2\text{O}$	---	No reaction	---
5	$\text{Fe}_3\text{O}_4@\text{SiO}_2\text{-BF}_3$ (5)	> 13 months	12 sec	89
6	$\text{Fe}_3\text{O}_4@\text{SiO}_2\text{-BF}_3$ (10)	> 13 months	6 sec	95
7	$\text{Fe}_3\text{O}_4@\text{SiO}_2\text{-BF}_3$ (15)	> 13 months	8 sec	90
8	$\text{Fe}_3\text{O}_4@\text{SiO}_2\text{-BF}_3$ (20)	> 13 months	8 sec	87

<sup>a</sup> The yields refer to the total isolated yield of 2-(4-chlorophenylazo)-1-naphthol and 4-(4-chlorophenylazo)-1-naphthol after adding fresh 4-chlorophenyl diazonium salt into basic 1-naphthol. <sup>b</sup> Silica phosphoric acid. <sup>c</sup> Silica chloride.

In this spectrum, the ethanolic OH and existing moisture in  $\text{BF}_3 \cdot \text{Et}_2\text{O}$  caused a broad O–H stretching band at wavenumber of  $3419 \text{ cm}^{-1}$ . The appearance of a new band at  $2289 \text{ cm}^{-1}$  clearly demonstrated  $\text{N}\equiv\text{N}$  stretching vibration and verified the formation of 4-chlorophenyl diazonium salt. The absorption bands of B–O and Si–O vibrations were observed at  $1442$  and  $1085 \text{ cm}^{-1}$ , respectively. Aromatic C–H bending vibrations, C–Cl and Fe–O stretching bands were revealed at  $829$ ,  $634$ , and  $586 \text{ cm}^{-1}$ , respectively.

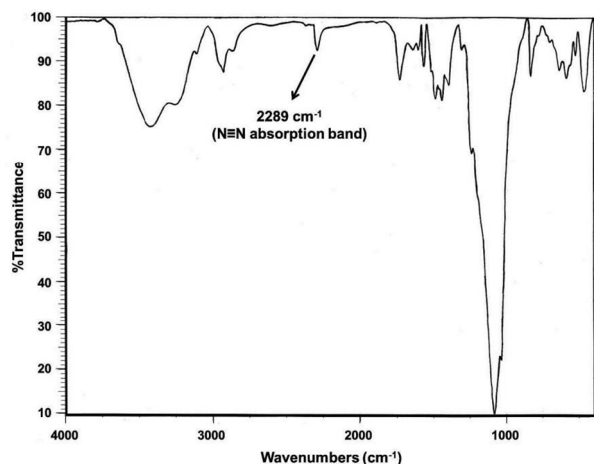
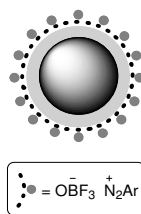


**Fig. 6** FT-IR spectrum of 4-chlorophenyl diazonium salt supported on  $\text{Fe}_3\text{O}_4@/\text{SiO}_2\text{-BF}_3$  MNPs.

According to this information, the structure of aryl diazonium salts supported on MNPs was guessed. Scheme 3 reveals that in this probable structure, aryl diazonium cations are located on the surface of negatively charged particles called  $\text{Fe}_3\text{O}_4$ -silica trifluoroborate nanoparticles. So, the presence of bulky anions and charge-charge interactions between nitrogen and boron atoms are the possible reasons of unusual stability of these salts.

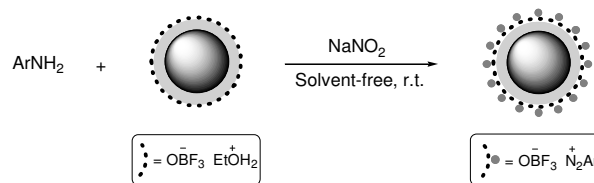


**Scheme 3** The probable structure of aryl diazonium salt supported on  $\text{Fe}_3\text{O}_4@/\text{SiO}_2\text{-BF}_3$  nanoparticles.

As a result, the high conversions of aniline derivatives to aryl diazonium salts and their long-term stability showed that the  $\text{Fe}_3\text{O}_4@/\text{SiO}_2\text{-BF}_3$  has strong and sufficient acidic sites, which are responsible for excellent performance in synthesis of aryl diazonium salts.

After optimization of the conditions, aniline derivatives including electron-withdrawing and electron-donating substituents were ground with  $\text{NaNO}_2$  and  $\text{Fe}_3\text{O}_4@/\text{SiO}_2\text{-BF}_3$  nanoparticles. Aryl diazonium salts were obtained in a very short time with an excellent conversion at room temperature (Scheme 4). Indeed, due to the high acidic strength of  $\text{Fe}_3\text{O}_4@/\text{SiO}_2\text{-BF}_3$  nanoparticles, the reaction was done so rapid that the substituent type could not effect on the time of

diazotization.



**Scheme 4** Diazotization of aromatic amines in the presence of  $\text{Fe}_3\text{O}_4@/\text{SiO}_2\text{-BF}_3$  nanoparticles.

It is important to note that  $\text{Fe}_3\text{O}_4@/\text{SiO}_2\text{-BF}_3$  in diazotization reaction acts as a two-function reagent, so that, on one side, its acidic protons convert the nitrite anions ( $\text{NO}_2^-$ ) in  $\text{NaNO}_2$  to nitrosonium cations ( $\text{NO}^+$ ) to promote diazotization and on the other side, its bulky anions cause the stability of aryl diazonium cations.

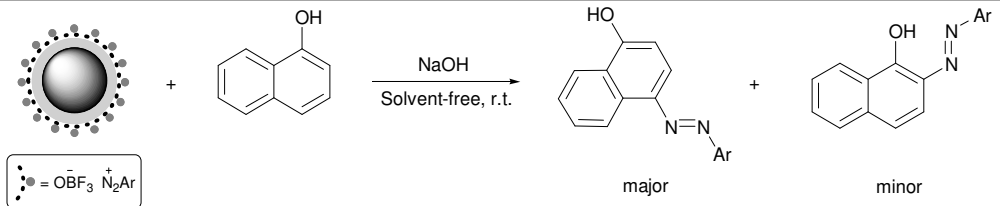
### Synthesis of arylazo-1-naphthol dyes

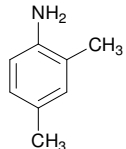
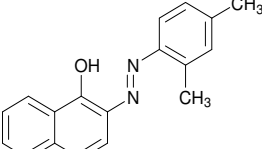
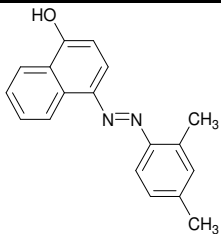
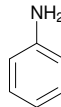
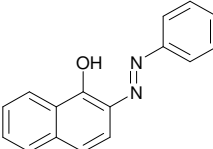
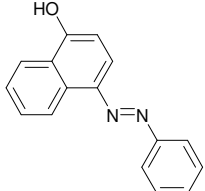
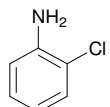
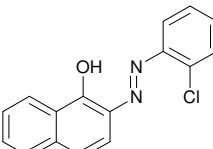
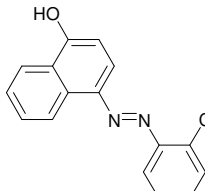
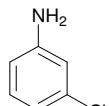
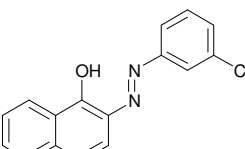
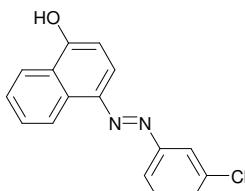
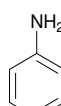
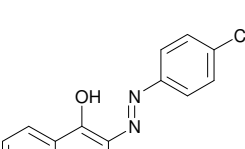
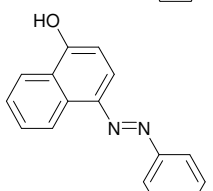
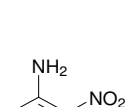
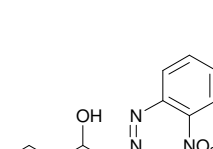
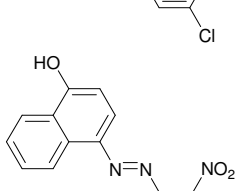
The most common synthetic route to the arylazo-1-naphthol compounds involves coupling of aryl diazonium salts with 1-naphthol in basic solution. Although using of water for preparation of 1-naphthoxide salt seems to be necessary, but like the previous step, using of water cause the formation of some phenoxide salt and its attack to diazonium salt to form phenolic azo dyes. To prevent this problem, the reaction was performed under solvent-free condition toward green chemistry. So, we ground solid 1-naphthol with some  $\text{NaOH}$  in a mortar. The moisture absorbed by the reaction mixture during the grinding seems to be sufficient for the formation of a homogeneous mixture. Moreover, the higher concentration of reactants in the absence of solvent at room temperature usually leads to more favourable kinetics than in solution.<sup>18</sup>

In this reaction, diazo coupling of aryl diazonium salts with 1-naphthoxide led to two products in which 4-arylazo-1-naphthol derivatives were the major products and 2-arylazo-1-naphthol derivatives got as the minor products. The resulted two main products were easily separated by flash column chromatography and identified by  $^1\text{H-NMR}$  and FT-IR spectroscopic methods. The molar ratios of these two dyes were determined from integral intensities of OH/NH signals in  $^1\text{H-NMR}$  spectrum (ratio 5:1 for 4-arylazo-1-naphthol to 2-arylazo-1-naphthol). Total yields of two products are shown in Table 2. It is also important that the electronic effects of aryl diazonium salt substituents do not play significant role in the rate of diazo coupling step. However, coupling reaction occurred rapidly regardless of substituent effects.

Totally, in this research we investigated the application of  $\text{Fe}_3\text{O}_4@/\text{SiO}_2\text{-BF}_3$  MNPs as a strong and useful solid acid reagent for synthesis of azo dyes based on 1-naphthol via a green procedure.

**Table 2** Solvent-free synthesis of arylazo-1-naphthol derivatives at room temperature.

					
Entry	Amine	2-Aryldiazo-1-naphthol (a')	4-Aryldiazo-1-naphthol (b')	Yield <sup>a</sup> (%)	MP <sub>found</sub> (Lit.) in a'/found (Lit.) in b' (°C)
1				92	181-183 (180.5-181) <sup>19</sup> / 176-178 (177-178) <sup>20</sup>
2				89	116-118/ 157-159 (159) <sup>20</sup>
3				93	127-129 (127.5-128) <sup>19</sup> / 173-175 (173) <sup>20</sup>
4				91	157-159 (156) <sup>19</sup> / 160-162 (162-163) <sup>20</sup>
5				90	116-118 (117-118) <sup>21</sup> / 201-203 (200) <sup>20</sup>
6				96	148-150 (151) <sup>19</sup> / 211-213 (211.5) <sup>20</sup>

7				87	184-186 (186) <sup>21</sup> / 138-140
8				89	137-139 (138) <sup>22</sup> / 207-209 (208) <sup>20</sup>
9				92	172-174/ 188-190 (189.5-190.5) <sup>20</sup>
10				90	152-154/ 228-230 (227.5-228) <sup>20</sup>
11				95	187-189 (187) <sup>21</sup> / 229-231 (229.5) <sup>20</sup>
12				85	216-218 (216) <sup>23</sup> / 258-260 (256- 257) <sup>20</sup>

<sup>a</sup> Total isolated yield of 2-arylazo-1-naphthols and 4-arylazo-1-naphthols after chromatography.

## Experimental

### Materials and apparatus

Chemicals and solvents were purchased from Merck and Sigma-Aldrich Companies. Melting points were obtained with a micro melting point apparatus (Electrothermal, Mk3) and are uncorrected. <sup>1</sup>H-NMR spectra were recorded on a Bruker DRX-400 Avance spectrometer. Tetramethyl silane (TMS) was used as an internal reference and CDCl<sub>3</sub> and DMSO-*d*<sub>6</sub> used as solvents. FT-IR spectra were run on a Nicolet Magna 550 spectrometer. The ultrasonic equipment used for the synthesis of MNPs (Fe<sub>3</sub>O<sub>4</sub>, Fe<sub>3</sub>O<sub>4</sub>@SiO<sub>2</sub>, and Fe<sub>3</sub>O<sub>4</sub>@SiO<sub>2</sub>-BF<sub>3</sub>) was a Sonica 2200ETH S3 SOLTEC ultrasonic bath (Italy) with a

working frequency of 40 KHz. XRD patterns were acquired using a Philips Xpert MPD diffractometer equipped with a Cu Kα anode (λ=1.54 Å) in the 2θ range from 10 to 80°. Magnetization of the samples was recorded as a function of the applied magnetic field sweeping between ±10 kOe at room temperature. All measurements were performed on a vibrating sample magnetometer device (Meghnatis Daghigh Kavir Co.; Kashan Kavir; Iran). The morphology of the synthesized samples was studied by a Mira II LMU Tescan FE-SEM made in Czech Republic. Elemental composition of three above mentioned MNPs was investigated by EDS spectroscopy (SAMX, France). The average size of Fe<sub>3</sub>O<sub>4</sub> and Fe<sub>3</sub>O<sub>4</sub>@SiO<sub>2</sub>-BF<sub>3</sub> MNPs was analyzed by TEM using a Philips CM120 with



a LaB6 cathode and accelerating voltage of 120 kV.

### Synthesis of $\text{Fe}_3\text{O}_4@/\text{SiO}_2\text{--BF}_3$ MNPs

The synthesis of  $\text{Fe}_3\text{O}_4$  nanoparticles was carried out according to the known procedure using chemical co-precipitation method by a little modification of the methodology already reported in the literature.<sup>24</sup> Briefly,  $\text{FeCl}_3\cdot 6\text{H}_2\text{O}$  (8.0 g, 0.0216 mol) and  $\text{FeCl}_2\cdot 4\text{H}_2\text{O}$  (3.5 g, 0.0108 mol) with molar ratio of 1:2, were dissolved in 38 mL of deoxygenated 0.4 M HCl solution. Then, 375 mL of deoxygenated 0.7 M ammonia solution was quickly added into the reaction mixture under sonication and nitrogen atmosphere. This resulted in immediate formation of a black precipitate of  $\text{Fe}_3\text{O}_4$  (magnetite). The sonication of magnetite dispersion was continued for 30 min. Finally, the precipitates were collected using an external magnetic field and washed for several times with distilled water and ethanol. The synthesized  $\text{Fe}_3\text{O}_4$  MNPs were suspended in 50 mL of distilled water for use in the next steps.

Modified Stöber sol-gel process,<sup>25</sup> was used for coating magnetite nanoparticles with a silica shell. Typically, 50 mL of magnetite suspended in water was added to 250 mL ethanol and sonicated at room temperature for 20 min under nitrogen flow. Then 11.85 mL PEG 200, 50 mL distilled water, 25 mL  $\text{NH}_3$  (28%) were added respectively, and after 15 min, 5 mL of TEOS was introduced into the suspension and the mixture was again sonicated for 6 h.  $\text{Fe}_3\text{O}_4@/\text{SiO}_2$  nanoparticles was centrifuged at 3000 rpm for 10 min, the solvent was discarded and nanoparticles were washed three times with water and then ethanol and dried in vacuum at room temperature.

In the final stage,  $\text{BF}_3\cdot \text{Et}_2\text{O}$  (0.45 mL) was added drop-wise to a slurry containing  $\text{Fe}_3\text{O}_4@/\text{SiO}_2$  core-shell nanoparticles (4.5 g) and ethanol (15 mL). The mixture was sonicated for 1 h at room temperature. The resulted suspension was filtered and dried at room temperature to obtain the brown solid named nano  $\text{Fe}_3\text{O}_4@/\text{SiO}_2\text{--BF}_3$  (10 wt%).

### Typical procedure for synthesis of arylazo-1-naphthol dyes

For synthesis of arylazo-1-naphthol derivatives, we mixed aromatic amines (2 mmol) with sodium nitrite (3 mmol) and  $\text{Fe}_3\text{O}_4@/\text{SiO}_2\text{--BF}_3$  nanoparticles (0.3 gr), respectively in a mortar with a pestle by rapid grinding. The progress of reaction was monitored by TLC (Ethyl acetate/n-Hexane). On the other side, for preparation of 1-naphthoxide salt, we ground 2 mmol of 1-naphthol and 10 mmol NaOH in the other mortar. Then, aryl diazonium salt was added to 1-naphthoxide salt and mixing and grinding resumed for a short time (about 3 min). After the completion of reaction and formation of two main products (2-arylazo-1-naphthol and 4-arylazo-1-naphthol), the mixture was washed by distilled water (3×10 mL) and then by acetone (4×5 mL). Two final products were separated by flash column chromatography with silica mesh of 230–400 (40–63  $\mu\text{m}$ ).

### Conclusion

$\text{Fe}_3\text{O}_4@/\text{SiO}_2\text{--BF}_3$  MNPs as a novel heterogeneous solid acid reagent was prepared by supporting of  $\text{BF}_3\cdot \text{Et}_2\text{O}$  on the surface of  $\text{Fe}_3\text{O}_4@/\text{SiO}_2$  core-shell nanoparticles and characterized by various methods. Then, some brilliant arylazo-1-naphthol derivatives were successfully synthesized by diazotization of

aniline derivatives in the presence of  $\text{Fe}_3\text{O}_4@/\text{SiO}_2\text{--BF}_3$  MNPs and their diazo coupling with 1-naphthol at room temperature. Using  $\text{Fe}_3\text{O}_4@/\text{SiO}_2\text{--BF}_3$  and solvent-free procedure caused the experimental simplicity, no use of special conditions such as liquid acids and low temperature, compatibility with environment, efficient yields, short reaction times and made this procedure attractive to synthesize a variety of these important dyes. The structure and stability of aryl diazonium salt supported on  $\text{Fe}_3\text{O}_4@/\text{SiO}_2\text{--BF}_3$  MNPs were studied, too.

### Acknowledgments

The authors are grateful to University of Kashan for supporting this work by Grant No. 159189/41.

### Notes and references

Department of Organic Chemistry, Faculty of Chemistry, University of Kashan, Kashan 87317-51167, Iran.

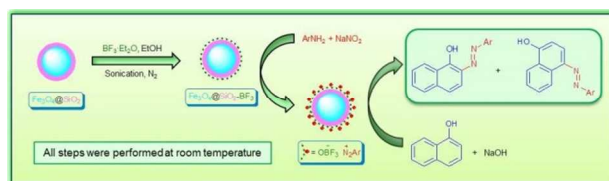
E-mail: bamoniri@kashanu.ac.ir

- (a) T. Kaicharla, S. R. Yetra, T. Roy and A. T. Biju, *Green Chem.*, 2013, **15**, 1608–1614; (b) M. V. Reddy and Y. T. Jeong, *Tetrahedron Lett.*, 2013, **54**, 3546–3549; (c) M. Özil and M. Canpolat, *Polyhedron*, 2013, **51**, 82–89; (d) Z. N. Siddiqui and T. Khan, *RSC Adv.*, 2014, **4**, 2526–2537; (e) J. Kamalraja and P. T. Perumal, *Tetrahedron Lett.*, 2014, **55**, 3561–3564; (f) D. Lanari, O. Rosati and M. Curini, *Tetrahedron Lett.*, 2014, **55**, 1752–1755.
- H. S. Freeman and A. T. Peters, *Colorants for Non-Textile Applications*, Elsevier Science B.V., Amsterdam, 2000.
- P. Gregory, *High Technology Applications of Organic Colorants*, Plenum, New York, 1991, Chapter 9.
- Y. Kubo, S. Maeda, S. Tokita and M. Kubo, *Nature*, 1996, **382**, 522–524.
- R. Steinsträsser and L. Pohl, *Angew. Chem., Int. Ed.*, 1973, **12**, 617–630.
- Y. He, X. Gu, M. Guo and X. Wang, *Opt. Mater.*, 2008, **31**, 18–27.
- S. Pieraccini, S. Masiero, G. P. Spada and G. Gottarelli, *Chem. Commun.*, 2003, **9**, 598–599.
- M. Tatsuta and T. Kitao, *Reagent for Detecting and Diagnosing Cancer*, Publication No. JP 01-207247 A, 1989.
- A. Aszalos, J. L. Weaver and P. S. Pine, *Methods of Using Azo Dyes and Their Derivatives*, US Patent No. 5,468,469, 1995.
- R. M. Christie, *Colour Chemistry*, Royal Society of Chemistry, Cambridge, 2001, Chapter 3.
- (a) A. B. Atar and Y. T. Jeong, *Tetrahedron Lett.*, 2013, **54**, 1302–1306; (b) F. Jing, B. Katryniok, E. Bordes-Richard and S. Paul, *Catal. Today*, 2013, **203**, 32–39; (c) Y. B. Huang and Y. Fu, *Green Chem.*, 2013, **15**, 1095–1111; (d) M. Billamboz, F. Mangin, N. Drillaud, C. Chevrin-Villette, E. Banaszak-Léonard and C. Len, *J. Org. Chem.*, 2014, **79**, 493–500; (e) C. Battilocchio, J. M. Hawkins and S. V. Ley, *Org. Lett.*, 2014, **16**, 1060–1063; (f) K. M. Hello, H. R. Hasan, M. H. Sauodi and P. Morgen, *Appl. Catal., A*, 2014, **475**, 226–234; (g) J. G. Hernández-Cortez, M. Manríquez, L. Lartundo-Rojas and E. López-Salinas, *Catal. Today*, 2014, **220–222**, 32–38.
- (a) J. H. Clark, *Catalysis of Organic Reactions by Supported Inorganic Reagents*, VCH, New York, 1994; (b) T. Okuhara, *Chem. Rev.*, 2002, **102**, 3641–3666.
- (a) A. K. Shah, K. J. Prathap, M. Kumar, S. H. R. Abdi, R. I. Kureshy, N. H. Khan and H. C. Bajaj, *Appl. Catal., A*, 2014, **469**, 442–450; (b) M. Korzec, P. Bartzak, A. Niemczyk, J. Szade, M. Kapkowski, P. Zenderowska, K. Balin, J. Lelatkó and J. Polanski, *J. Catal.*, 2014, **313**, 1–8; (c) Z. Dong, X. Le, X. Li, W. Zhang, C. Dong and J. Ma, *Appl. Catal., B*, 2014,

- 158–159, 129–135; (d) X. Le, Z. Dong, W. Zhang, X. Li and J. Ma, *J. Mol. Catal. A: Chem.*, 2014, **395**, 58–65; (e) T. R. Mandlimath, B. Umamahesh and K. I. Sathiyarayanan, *J. Mol. Catal. A: Chem.*, 2014, **391**, 198–207.
- 14 L. H. Reddy, J. L. Arias, J. Nicolas and P. Couvreur, *Chem. Rev.*, 2012, **112**, 5818–5878.
- 15 (a) Y. H. Liu, J. Deng, J. W. Gao and Z. H. Zhang, *Adv. Synth. Catal.*, 2012, **354**, 441–447; (b) X. Zhang, X. He, L. Chen and Y. Zhang, *J. Mater. Chem.*, 2012, **22**, 16520–16526; (c) X. Jin, K. Zhang, J. Sun, J. Wang, Z. Dong and R. Li, *Catal. Commun.*, 2012, **26**, 199–203; (d) H. J. Xu, X. Wan, Y. Y. Shen, S. Xu and Y. S. Feng, *Org. Lett.*, 2012, **14**, 1210–1213; (e) G. M. Ucoski, F. S. Nunes, G. F. Silva, Y. M. Idemori and S. Nakagaki, *Appl. Catal., A*, 2013, **459**, 121–130; (f) F. Nemati, R. Saedirad, *Chin. Chem. Lett.*, 2013, **24**, 370–372; (g) S. Wang, Z. Zhang, B. Liu and J. Li, *Catal. Sci. Technol.*, 2013, **3**, 2104–2112; (h) M. R. Nabid, Y. Bide and M. Niknezhad, *ChemCatChem*, 2014, **6**, 538–546; (i) F. Zhang, M. Chen, X. Wu, W. Wang and H. Li, *J. Mater. Chem. A*, 2014, **2**, 484–491; (j) R. K. Sharma, Y. Monga and A. Puri, *J. Mol. Catal. A: Chem.*, 2014, **393**, 84–95; (k) E. Kolvari, N. Koukabi and O. Armandpour, *Tetrahedron*, 2014, **70**, 1383–1386.
- 16 (a) B. F. Mirjalili, A. Bamoniri and A. Akbari, *Tetrahedron Lett.*, 2008, **49**, 6454–6456; (b) B. F. Mirjalili, A. Bamoniri, M. A. Karimi Zarchi and H. Emtiazi, *J. Iran. Chem. Soc.*, 2010, **7**, 95–99; (c) B. F. Mirjalili, A. Bamoniri and A. Akbari, *J. Iran. Chem. Soc.*, 2011, **8**, 135–140; (d) A. Bamoniri, A. Ghorbani-Choghamarani and B. F. Mirjalili, *Phosphorus Sulfur Silicon Relat. Elem.*, 2011, **186**, 381–388; (e) A. Bamoniri, B. F. Mirjalili, A. A. Jafari and F. Abasaltian, *Iran. J. Catal.*, 2012, **2**, 73–76; (f) B. F. Mirjalili, A. Bamoniri and M. A. Mirhoseini, *Chem. Heterocycl. Compd.*, 2012, **48**, 856–860; (g) B. F. Mirjalili, A. Bamoniri and L. Zamani, *Sci. Iran.*, 2012, **19**, 565–568; (h) A. Bamoniri, B. F. Mirjalili and S. Nazemian, *Curr. Chem. Lett.*, 2013, **2**, 27–34; (i) A. Bamoniri, B. F. Mirjalili and S. Nazemian, *J. Iran. Chem. Soc.*, 2014, **11**, 653–658.
- 17 K. Wilson and J. H. Clark, *Chem. Commun.*, 1998, 2135–2136.
- 18 (a) F. Toda and K. Tanaka, *Chem. Rev.*, 2000, **100**, 1025–1074; (b) K. Tanaka, *Solvent-Free Organic Synthesis*, John Wiley & Sons, New York, 2003.
- 19 L. N. Ogoleva and B. I. Stepanov, *Ž. Org. Chim.*, 1965, **1**, 2083–2086.
- 20 K. J. Morgan, *J. Chem. Soc.*, 1961, 2151–2159.
- 21 G. Charrier and G. Ferreri, *Gazz. Chim. Ital.*, 1914, **44**, 234.
- 22 W. R. Brode and L. E. Herdle, *J. Org. Chem.*, 1941, **6**, 713–721.
- 23 E. Bamberger, *Chem. Ber.*, 1897, **30**, 513–516.
- 24 M. Emadi, E. Shams and M. K. Amini, *J. Chem.*, 2013, Article No. 787682, DOI:10.1155/2013/787682.
- 25 W. Stöber, A. Fink and E. Bohn, *J. Colloid Interface Sci.*, 1968, **26**, 62–69.

# Nano-Fe<sub>3</sub>O<sub>4</sub> encapsulated-silica supported boron trifluoride as a novel heterogeneous solid acid for solvent-free synthesis of arylazo-1-naphthol derivatives

Abdolhamid Bamoniri and Naimeh Moshtael-Arani



Fe<sub>3</sub>O<sub>4</sub>@SiO<sub>2</sub>-BF<sub>3</sub> nanoparticles were prepared as a novel solid acid, and effectively applied for solvent-free synthesis of arylazo-1-naphthols at room temperature.